PNAS RESEARCH ARTICLE | GENETICS

DNA polymerase delta governs parental histone transfer to DNA replication lagging strand

Congcong Tian[a,1], Qin Zhang[b,1], Jing Jia[c,1], Jiaqi Zhou[a,1], Ziwei Zhang[a,1], Srinivasu Karri[c], Jiuhang Jiang[a,d], Quinn Dickinson[c], Yuan Yao[a], Xiaorong Tang[a,e], Yuxin Huang[a,d], Ting Guo[a,f,g], Ziwei He[h], Zheng Liu[h], Yuan Gao[i], Xinran Yang[a], Yuchun Wu[a,j], Kui Ming Chan[k,l], Daoqin Zhang[m], Junhong Han[b,2], Chuanhe Yu[c,2], and Haiyun Gan[a,2]

Edited by Douglas Koshland, University of California, Berkeley, CA; received January 17, 2024; accepted April 1, 2024

Chromatin replication is intricately intertwined with the recycling of parental histones to the newly duplicated DNA strands for faithful genetic and epigenetic inheritance. The transfer of parental histones occurs through two distinct pathways: leading strand deposition, mediated by the DNA polymerase ε subunits Dpb3/Dpb4, and lagging strand deposition, facilitated by the MCM helicase subunit Mcm2. However, the mechanism of the facilitation of Mcm2 transferring parental histones to the lagging strand while moving along the leading strand remains unclear. Here, we show that the deletion of Pol32, a nonessential subunit of major lagging-strand DNA polymerase δ, results in a predominant transfer of parental histone H3–H4 to the leading strand during replication. Biochemical analyses further demonstrate that Pol32 can bind histone H3–H4 both in vivo and in vitro. The interaction of Pol32 with parental histone H3–H4 is disrupted through the mutation of the histone H3–H4 binding domain within Mcm2. Our findings identify the DNA polymerase δ subunit Pol32 as a critical histone chaperone downstream of Mcm2, mediating the transfer of parental histones to the lagging strand during DNA replication.

parental histone transfer | Pol32 | DNA polymerase δ | histone chaperone | epigenetic inheritance

Significance

As faithful DNA replication is a crucial process for genetic inheritance, the accurate copying of epigenetic information is vital for maintaining cell lineage. It is well known that DNA polymerases are responsible for genomic DNA duplication. In this study, we have identified that Pol δ, one of the DNA polymerases, serves as a key chaperone for transferring parental histones to the lagging strand during DNA replication, assuring the faithful inheritance of epigenetic information carried by parental histone posttranslational modifications to the daughter cells. This finding reveals an exquisite process that Pol δ facilitates parental histone inheritance while replicating the lagging DNA strands.

Recent studies have highlighted the crucial role of chromatin structure in gene regulation (1). In eukaryotic cells, the nucleosome serves as the basic unit of chromatin, comprising approximately 150 base pairs of DNA and a histone octamer with two copies of each of H2A, H2B, H3, and H4. Chromatin organization is not uniform along the chromosome; certain regions are densely packaged as heterochromatin, while others are loosely arranged as euchromatin (2, 3).

The replication of chromatin is intricately linked with DNA replication, yet a significant knowledge gap persists regarding the precise mechanisms governing chromatin inheritance during this process. Unlike the H2A–H2B dimers, which can be readily removed and turn over quickly during transcription, the H3–H4 tetramers are more stable and emerge as an ideal vector for preserving epigenetic memory across cell divisions (4, 5). Experimental evidence of the local recycling of histone H3–H4 tetramers during DNA replication supports this hypothesis (6). In line with this, the observation that the core histone component H3–H4 tetramer remains intact during DNA replication further reinforces this concept (7). As the replication fork advances, nucleosomes undergo the disassembly process to facilitate the passage of the replisome. Subsequently, the newly synthesized DNA daughter strands recycle parental histones from the parental strand and recruit newly synthesized histones, thereby restoring nucleosome structure. This nucleosome assembly process signifies the initial step in transferring epigenetic information from parent to daughter cells (8, 9). The faithful transfer and restoration of posttranslational histone modifications, carried by the parental histone H3–H4, are crucial for maintaining cell identity through cell division (3, 10).

Several newly synthesized H3–H4 chaperones, defined by both their binding to H3–H4 tetramers and roles in nucleosome assembly (8, 9), have been identified, including CAF1, RTT106, and ASF1. These chaperones not only play essential roles in chromatin replication, but also in the DNA damage repair process (11, 12). However, compared to the assembly of new H3–H4, the recycling process of parental histone poses greater challenges due to methodological difficulties. Biochemical analysis has shown that Mcm2, a subunit of the replicative helicase MCM, contains a histone-binding motif (HBM) allowing it to bind to the histone H3–H4 tetramer in yeast (13). Subsequent structural analysis revealed that the MCM–H3–H4 interaction is conserved among eukaryotic cells (14). Through genome-wide sequencing analysis tools, such as eSPAN (enrichment and sequencing of protein-associated nascent DNA) (15, 16), as

Author contributions: C.T., Y.Y., J.H., C.Y., and H.G. designed research; C.T., Q.Z., J. Jia, Z.Z., S.K., J. Jiang, Q.D., X.T., Y.H., T.G., and X.Y. performed research; J.Z., Z.H., Z.L., Y.W., and H.G. analyzed data; and C.T., Q.D., Y.G., K.M.C., D.Z., and C.Y. wrote the paper.

The authors declare no competing interest.

This article is a PNAS Direct Submission.

[1]C.T., Q.Z., J. Jia, J.Z., and Z.Z. contributed equally to this work.

[2]To whom correspondence may be addressed. Email: hjunhong@scu.edu.cn, yu000479@umn.edu, or hy.gan@siat.ac.cn.

This article contains supporting information online at https://www.pnas.org/lookup/suppl/doi:10.1073/pnas.2400610121/-/DCSupplemental.

Published May 7, 2024.

depicted in *SI Appendix*, Fig. S1*A*, several mediators of parental histone H3–H4 transfer have been identified through the altered balance of leading and lagging strand inheritance while perturbed (15, 17, 18). The DNA polymerase ε subunit Dpb3/Dpb4 has been shown to bind to H3–H4 in vitro and mediates the transfer of parental histone H3–H4 tetramers to the leading strand. Meanwhile, the Mcm2-Ctf4-Polα axis facilitates the transfer of parental histones to the lagging strand. Mutations in the HBM of Mcm2 or mutations disrupting the CMG-Ctf4-Polα interaction result in defective transfer of parental histone H3–H4 tetramers to the lagging strand (15, 17–19). Moreover, Polα has also been shown to directly bind to histone H3–H4 tetramers and facilitates lagging strand transfer (19, 20). Although mutations altering these parental histones transfer only exhibit a minor phenotype in chromatin stability in budding yeast model (13, 17, 21), there are profound impacts on the differentiation of mouse embryonic stem cells and more importantly mouse embryonic development (22–24).

However, the disruption of both Dpb3/Dpb4 and Mcm2-Ctf4-Polα pathways does not impede cell growth (21), suggesting the presence of an additional regulatory mechanism compensating for these two canonical pathways. In this study, we found that the nonessential DNA polymerase δ subunit, Pol32, binds to histone H3–H4 both in vivo and in vitro. Depletion of Pol32 leads to a predominant transfer of parental histone H3–H4 to the replication leading strand. Furthermore, biochemical analysis shows that the binding of Pol32 to parental histones is dependent on Mcm2. In conclusion, we identify DNA polymerase δ as a key histone chaperone downstream of Mcm2, mediating the transfer of parental histone to the lagging strand.

Results

Pol32 Is a Parental H3–H4 Histone Chaperone. Our previous work has shown that the strand bias effect is more pronounced when disrupting the Mcm2–H3–H4 interaction (*mcm2-3A* mutant) than eliminating the Pol1 (polymerase1)–H3–H4 interaction (*pol1-2A2* mutant) (*SI Appendix*, Fig. S1 *B* and *C*) (18, 19). This observation implies the presence of additional receptors for parental H3–H4 on the replication lagging strand. In yeast, newly deposited H3–H4 is typically marked with a H3K56ac modification, which is gradually removed by histone deacetylase during later S/G2 phases (25, 26). Subsequently, histone methyltransferases add methylation modifications to the nucleosomes (27). To identify candidate factors that changed the parental histone transfer pattern, we deleted several nonessential components involved in lagging strand replication (*SI Appendix*, Fig. S1*D*) and used H3K4me3-specific antibodies to track parental histone H3–H4 with the eSPAN method (Procedure see *SI Appendix*, Fig. S1*A*) (16–18). Pol32, the human homolog of POLD3, emerged from this screening as a key regulator. Compared to a slightly lagging strand bias of the WT control, the H3K4me3 eSPAN of *pol32Δ* exhibited a strong leading strand bias in HU (hydroxyurea)-treated early S phase cells (Fig. 1 *A*–*C*). The magnitude of this strand bias is comparable to that observed in the *mcm2-3A* mutant and is considerably stronger than in the *pol1-2A2* mutant (*SI Appendix*, Fig. S1 *B* and *C*). Meanwhile, the H3K56ac eSPAN of *pol32Δ* showed a pronounced lagging strand bias (Fig. 1 *A*–*C*), reinforcing the conclusion that Pol32 participates in the deposition of parental histone H3–H4 on the replication lagging strand. Further analysis of the H3K4me3 eSPAN without HU treatment still displayed a clear leading strand bias (*SI Appendix*, Fig. S1 *E* and *F*). Taken together, we found that Pol32 is involved in parental histone transfer.

To better understand the mechanisms of which Pol32 regulates parental histone transfer, without relying on the histone modification marks, we adapted the Recombination-Induced Tag Exchange system (6, 28) to mark all the parental histones with a HA (hemagglutinin) tag. Then recombination is induced prior to early S phase release to tag the new histones with T7 (Fig. 1*D*). With this system, we confirmed that H3–HA (parental) and H3–T7 (new) eSPAN revealed a distinct leading and lagging strand pattern across all of the genomic origins of replication (Fig. 1*E*). This pattern clearly contrasts with the lack of a clear bias in the WT control for both H3–HA and H3–T7 eSPAN (Fig. 1*E*). These findings collectively support the involvement of Pol32 in transferring parental histone H3–H4 to the replication lagging strand.

It has been shown that the Dpb3/Dpb4 of Pol ε and catalytic subunit of Polα can directly bind to histone H3–H4 tetramers (13, 19). However, it remains unknown whether Pol δ can bind to H3–H4. To test this, we then performed the Pol32 immunoprecipitation in DNase I digested chromatin and observed its interaction with H3 and H4 within the cell (Fig. 1*F*). Mcm2, which has been reported to bind H3–H4 (13, 14), served as the immunoprecipitation positive control (Fig. 1*F*). We further confirmed the Pol32–H3–H4 interaction is direct, by using in vitro purified Pol32 and H3–H4 tetramers (Fig. 1*G*). These findings suggest that Pol32 can act as a receptor or chaperone for parental H3–H4, to facilitate their assembly onto lagging strands.

Pol32 Receives Parental H3–H4 from Mcm2 and Transfers It to DNA Replication Lagging Strand. Next, we asked whether the relationship between Mcm2 and Pol32 in parental histone H3–H4 transfer is parallel or sequential at the replication fork. To test this, we conducted Pol32 immunoprecipitation in both WT and *mcm2-3A* strains. Compared to WT cells, the amount of H3–H4 pulled down by Pol32 significantly decreased under the *mcm2-3A* mutant context (Fig. 2*A*). Importantly, the Pol32-coprecipitated H3K4me3 (likely parental histone) also decreased, while the Pol32-bound H3K56ac (likely free histone) remained unchanged in the *mcm2-3A* mutant (Fig. 2*A*). These data suggest that the binding of Pol32 to parental histone H3–H4 is dependent on Mcm2, supporting the idea that parental histone H3–H4 is transferred from Mcm2 to Pol32.

We then explored whether Pol32 could interact with Mcm2 and whether this interaction depends on H3–H4. Coimmunoprecipitation experiments unveiled a robust interaction between Pol32 and WT Mcm2, whereas the interaction was diminished with the histone-binding mutant *mcm2-3A* (Fig. 2*B*). These data indicated that the Mcm2-Pol32 interaction is partially dependent on their association with H3–H4. Consistently, our in vitro binding assay with purified proteins also showed that the interaction between Pol32 and Mcm2 is stronger in the presence of H3–H4 (Fig. 2*C*), suggesting that Mcm2 and Pol32 can directly bind to each other, and the H3–H4 tetramer can mediate and enhance their interaction. These findings support a parental H3–H4 tetramer handoff model from Mcm2 to Pol32 (Fig. 2*D*).

Next, we asked whether the replisome hub protein Ctf4 also plays a role in the Pol32–Mcm2 interaction. Co-IP experiments showed that the interaction of Pol32 to H3K4me3 was slightly reduced (Fig. 2*E*), whereas the interaction with Mcm2 remained unaffected in *ctf4Δ* cells (Fig. 2*F*). In the Co-IP experiment involving the *ctf4-4E* mutant (disrupting the Ctf4-Pol1 interaction) (29), we observed little changes in both Pol32–Mcm2 and Pol32–H3–H4 interactions (Fig. 2 *E* and *F*). Altogether, the replisome hub protein Ctf4 has an additional role in supporting Pol32 in parental histone transfer; however, the interaction between Mcm2 and Pol32 is independent of Ctf4.

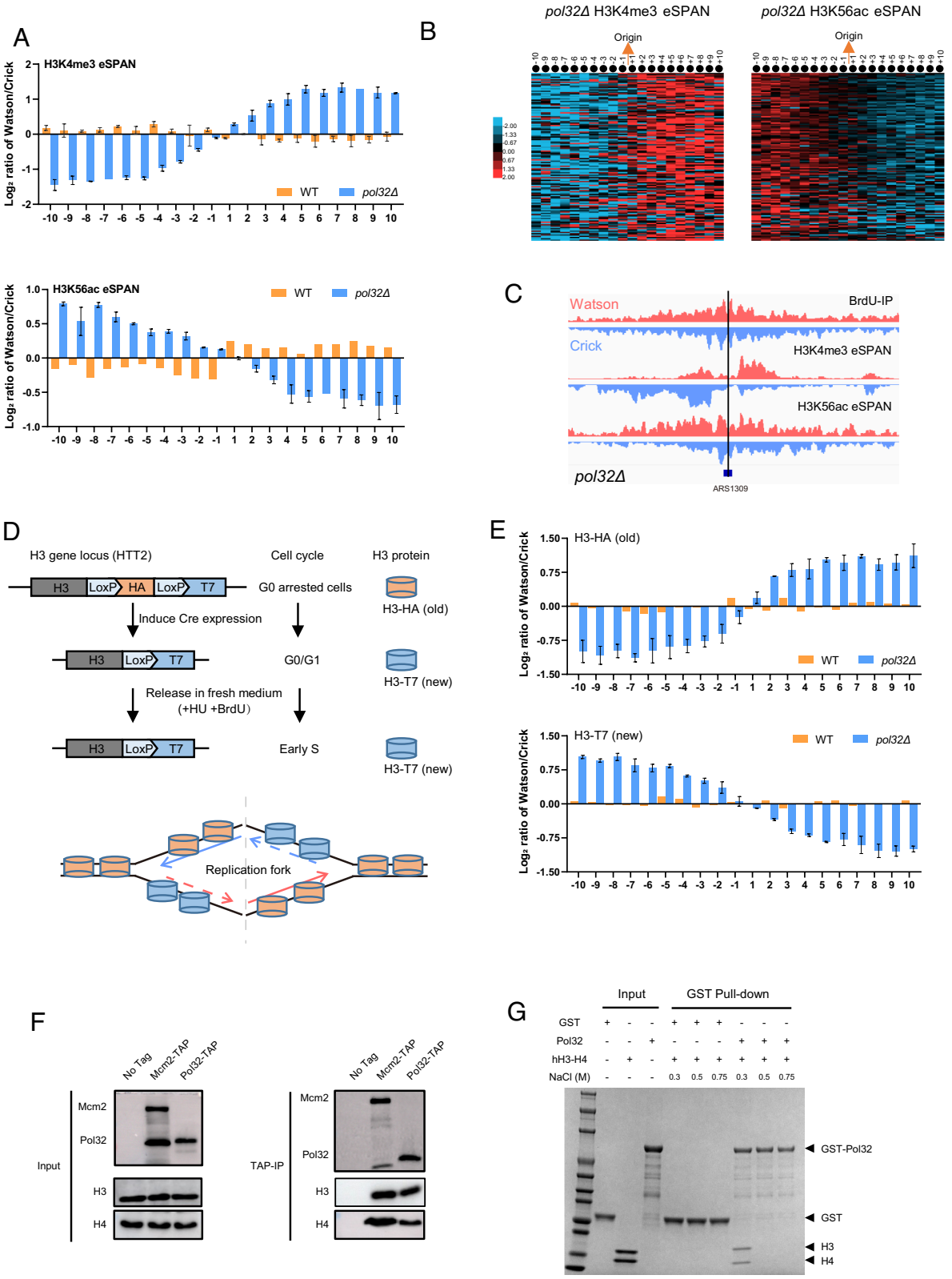

Fig. 1. Pol32 transfers parental histone H3–H4 to lagging strands. (*A*) The average bias ratio of H3K4me3 (*Upper*) and H3K56ac (*Lower*) eSPAN signal at each of the 10 nucleosomes flanking the early replication origins in WT and *pol32Δ* cells. For cell culture, alpha-factor arrested G1 cells were released into medium containing HU (200 mM) and BrdU for 45 min. The sample treatment following *SI Appendix*, Fig. S1*A*. (*B*) Heatmap showing the bias ratio and pattern of H3K4me3 (*Left*) and H3K56ac (*Right*) eSPAN signal at each nucleosome flanking the early replication origins in *pol32Δ* cells. (*C*) Snapshot of BrdU-IP-ssSeq, H3K4me3, and H3K56ac eSPAN peaks surrounding the ARS1309 origin in *pol32Δ* cells. (*D*) Experimental design to track the parental H3 with HA-tag (H3–HA) and newly synthesized H3 with T7-tag (H3-T7). The experimental procedure following previous publications (17, 28). (*E*) The average bias of H3–HA (*Upper*) and H3-T7 (*Lower*) eSPAN signal at the early replication origins in WT and *pol32Δ* cells. (*F*) In vivo interaction of Pol32 with H3–H4. TAP-tagged Pol32 (Pol32-TAP) was pulled down from yeast cell lysate with IgG beads. Copurified proteins were separated by SDS-PAGE and detected with specific antibodies. Cells without Pol32-TAP expression served as a negative control. (*G*) Immunoprecipitation (pull-down) recombinant hH3.1–H4 (human) tetramers by recombinant glutathione S-transferase (GST)-Pol32 or GST protein. Bound proteins were detected by Coomassie Brilliant Blue (CBB) staining.

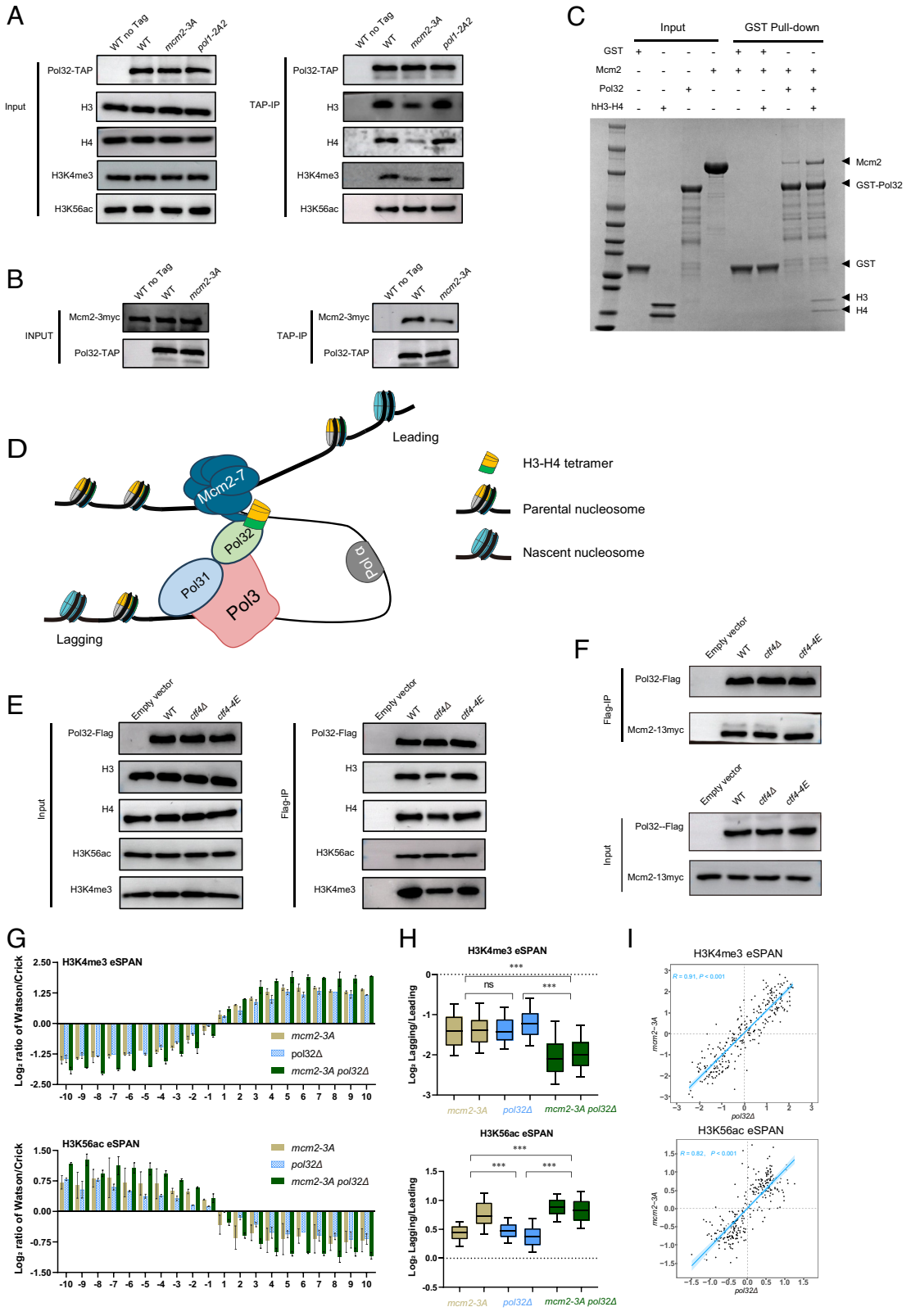

Fig. 2. Pol32 receives parental histones from Mcm2. (*A*) Analysis of Pol32-TAP-associated proteins from WT, *mcm2-3A,* and *pol1-2A2* mutant cells. (*B*) Analysis of the Pol32–Mcm2 interaction by Pol32-TAP purification in WT and *mcm2-3A* mutant cells. (*C*) H3–H4 tetramers promote Mcm2-Pol32 interaction. To assess the effect of H3–H4 on the interaction between Mcm2 and Pol32, Mcm2 was incubated with or without H3–H4, and then, the products were added into beads bearing GST-Pol32 or GST proteins (negative control). The pull-down assay was performed in buffer containing 500mM NaCl. (*D*) Interaction model of Mcm2, H3–H4, and Pol32 at the replication fork. (*E* and *F*) *ctf4Δ* reduces the interaction of parental histones (H3K4me3 as a surrogate) with Pol32 (*E*), but does not interfere with the Mcm2-Pol32 interaction (*F*). Plasmids (pRS423-Pol32-3×Flag or empty vector) were transfected into WT, *ctf4Δ,* and *ctf4-4E* strains. Pol32-Flag was isolated by immunoprecipitation, and its associated proteins were monitored by immunoblotting. (*G*) Average eSPAN bias of H3K4me3 (*Upper*) and H3K56ac (*Lower*) at each nucleosome flanking the early replication origins in *mcm2-3A*, *pol32Δ,* and *mcm2-3A pol32Δ* cells. The data displayed in the box filled with grids have been shown in Fig. 1*A*. (*H*) Box plots showing the ratio of sequencing reads at lagging over leading strands of eSPAN signal around each early replication origin in *mcm2-3A*, *pol32Δ,* and *mcm2-3A pol32Δ* cells. Two replicates were performed. (*I*) eSPAN bias pattern of H3K4me3 (*Upper*) and H3K56ac (*Lower*) in *pol32Δ* strongly correlated with that of *mcm2-3A*.

In conjunction with the biochemical analyses, we also employed the parental and new histone eSPAN to investigate the Mcm2-Pol32 interaction. The H3K4me3 (parental histone) eSPAN profiles of *mcm2-3A* and *pol32Δ* single mutants exhibited a similar strong leading bias pattern (Fig. 2 *G* and *H* and *SI Appendix*, Fig. S2 *A* and *B*). Moreover, the strand bias exhibited in the *mcm2-3A* and *pol32Δ* cells at all the replication origins are highly correlated (Fig. 2*I*). Importantly, combinations of *mcm2-3A* and *pol32Δ* mutants displayed synergistic effect compared to the single mutants in the H3K4me3 (parental histone) eSPAN analysis (Fig. 2 *G* and *H* and *SI Appendix*, Fig. S2 *A* and *B*). Meanwhile, the H3K56ac (new histone) eSPAN revealed a reciprocal pattern to that of the parental histone (Fig. 2 *G* and *H* and *SI Appendix*, Fig. S2 *A* and *B*), further solidifying the H3K4me3 (parental histone) results. These eSPAN analyses together with the biochemical data support a model whereby Mcm2 initially receives parental histone H3–H4 and subsequently transfers parental histones to Pol32 on the replication lagging strand (Fig. 2*D*). However, a proportion of the parental histone receipt by Pol32 is independent of Mcm2.

Pol1 Is a Pol32-Downstream Chaperone in the Parental Histone H3–H4 Transfer Pathway. We next sought to explore the relationship between Pol1 and Pol32 in the parental histone H3–H4 transfer pathway. Within the *pol1-2A2* (histone-binding mutant) context, Pol32 exhibited similar binding ability to H3–H4, H3K4me3, and H3K56ac when compared to the WT (Fig. 2*A*). Furthermore, we found that in the absence of Pol32, the interaction of Pol1 with H3K4me3-H4 was reduced, while the interaction with H3K56ac-H4 remained unchanged (Fig. 3*A*). We also conducted an in vitro binding assay with purified proteins and found that histone H3–H4 promotes the interaction between Pol32 and Pol1 (Fig. 3*B*). This is further supported by the in vivo result that Pol1–Pol32 interaction was weakened by the *pol1-2A2* mutation, which eliminates the H3–H4 binding capability of Pol1 (Fig. 3*C*). Previous studies have identified the domains responsible for the Pol1–Pol32 interaction: Pol1 278-532a.a. (in fission yeast) and Pol32 270 to 309a.a. (30, 31). Deletion of either of two domains dramatically decreased the interaction between Pol1 and Pol32 (we specifically deleted the 278 to 348 region of Pol1 due to essential catalytic function located in Pol1 349 to 532a.a. region), without affecting the interaction between Pol32 and H3–H4 (Fig. 3*D* and *SI Appendix*, Fig. S3*A*). Moreover, disrupting the interaction of Pol1 with Pol32 (*pol32Δ270-309*) does not affect its interaction with H3–H4 (Fig. 3*D* and *SI Appendix*, Fig. S3*B*). Consistently, the parental histone transfer remained affected, as the H3K4me3 eSPAN of *pol32Δ270-309* cells resembled the WT exhibiting a slight lagging strand bias (Fig. 3*E*). These results together suggest that the H3–H4 tetramer bridging, rather than the Pol1–Pol32 direct interaction, is crucial for the parental histone transfer pathway.

Additionally, the Pol1 histone-binding mutant (*pol1-2A2*) exhibited a much smaller strand bias on both H3K4me3 and H3K56ac eSPAN, than the *pol32Δ* single or *pol1-2A2 pol32Δ* double mutants (Fig. 3*F*). Meanwhile, the *pol32Δ* single and *pol1-2A2 pol32Δ* double mutants exhibit comparable histone transfer patterns, for both H3K4me3 and H3K56ac eSPAN (Fig. 3*F*). Moreover, the *pol1-2A2* and *pol32Δ* cells exhibit a strong correlation for both parental and new histone eSPAN (Fig. 3*G*). Overall, our eSPAN results indicate that Pol1 receives parental histone H3–H4 from Pol32 and transfers it to the replication lagging strand.

To provide a more complete view of the lagging strand transfer pathway, we conducted Mcm2 immunoprecipitation in WT, *pol32Δ* and *pol1-2A2* strains. The interaction between Mcm2 and H3–H4 remained unaffected in *pol32Δ* and *pol1-2A2* strains (*SI Appendix*, Fig. S3*C*). Furthermore, we also performed Pol1 immunoprecipitation in both WT and *mcm2-3A* strains. Compared to WT cells, the amount of H3–H4 pulled down by Pol1 significantly decreased under the *mcm2-3A* mutant context (*SI Appendix*, Fig. S3*D*). These results further suggest that Mcm2 acts upstream of Pol32, with Pol1 functioning downstream in the lagging strand transfer pathway.

The Histone Chaperone Function of Pol32 Is Independent of PCNA Interaction and DNA Binding Capability. Furthermore, as Pol32 contains a PIP (PCNA interaction protein-box) motif at the C-terminal (33), we conducted the H3K4me3 eSPAN analysis of *pol32-2A* (PIP motif mutation: Pol32-F344A, F345A), and observed no bias (*SI Appendix*, Fig. S3*E*), indicating that the histone chaperone function of Pol32 is independent of its interaction with PCNA.

It has been shown that Pol32 functions as the processivity factor for DNA polymerase δ and facilitates its localization to the nucleus (34). It is possible that Pol32 also harbors DNA binding ability. Indeed, we observed a notable Pol32–DNA shift in the DNA binding assay (*SI Appendix*, Fig. S4*A*). However, supplementing additional DNA did not affect the interaction between Pol32 and H3–H4 (*SI Appendix*, Fig. S4*B*). These analyses collectively suggest that Pol32 indeed possesses DNA binding capability, and importantly, this domain does not impede its histone chaperone functions.

Pol32 Deletion Leads to Chromatin Instability. Finally, we sought to further dissect the phenotypic function of Pol32. When grown within a rich growth medium, neither the *pol32Δ* mutant nor its combination with other mutants defective in parental histone transfer exhibit clear growth defects (*SI Appendix*, Fig. S5*A*). However, under replication stress conditions, for example with HU or camptothecin (CPT) treatment, they exhibit enhanced sensitivity (*SI Appendix*, Fig. S5*A*). This observed phenotype aligns with the well-established role of Pol32 in the DNA repair process (30, 35, 36). Interestingly, we did not observe any additive effect when combining *pol32Δ* with mutants affecting lagging strand parental histone transfer chaperones. Chromatin instability is a typical outcome of mutations in histone chaperones, and it has been shown that *pol32Δ* induces chromatin instability at both HML and telomeric regions through URA3/FOA analysis (37). To gain a deeper insight into its impact, we employed a more sensitive CRASH (Cre-reported altered states of heterochromatin) system (38) to investigate whether *pol32Δ* influences gene silencing in the HML locus (*SI Appendix*, Fig. S5*B*). Briefly, Cre is inserted to the HML locus, usually silenced within yeast. Cre would be derepressed and recombine the red fluorescent protein, green fluorescent protein (RFP-GFP) cassette once the silencing at the HML locus was lost, resulting in GFP expression. Thus, the ratio of the loss of silencing can be measured by the percentage of the cells expressing GFP. We found that *pol32Δ* leads to a onefold increase in the loss of silencing (*SI Appendix*, Fig. S5*C*), suggesting that Pol32 deletion leads to chromatin instability.

Discussion

In this study, we have identified the DNA polymerase δ subunit Pol32 as a key regulator of parental histone H3–H4 transfer to the DNA replication lagging strand. Using both in vivo and in vitro biochemical analyses, we showed that Pol32 can directly bind to histone H3–H4. Furthermore, we gained insight into the functional mechanism by showing that Pol32 operates downstream of Mcm2 and upstream of DNA Pol1, in the parental

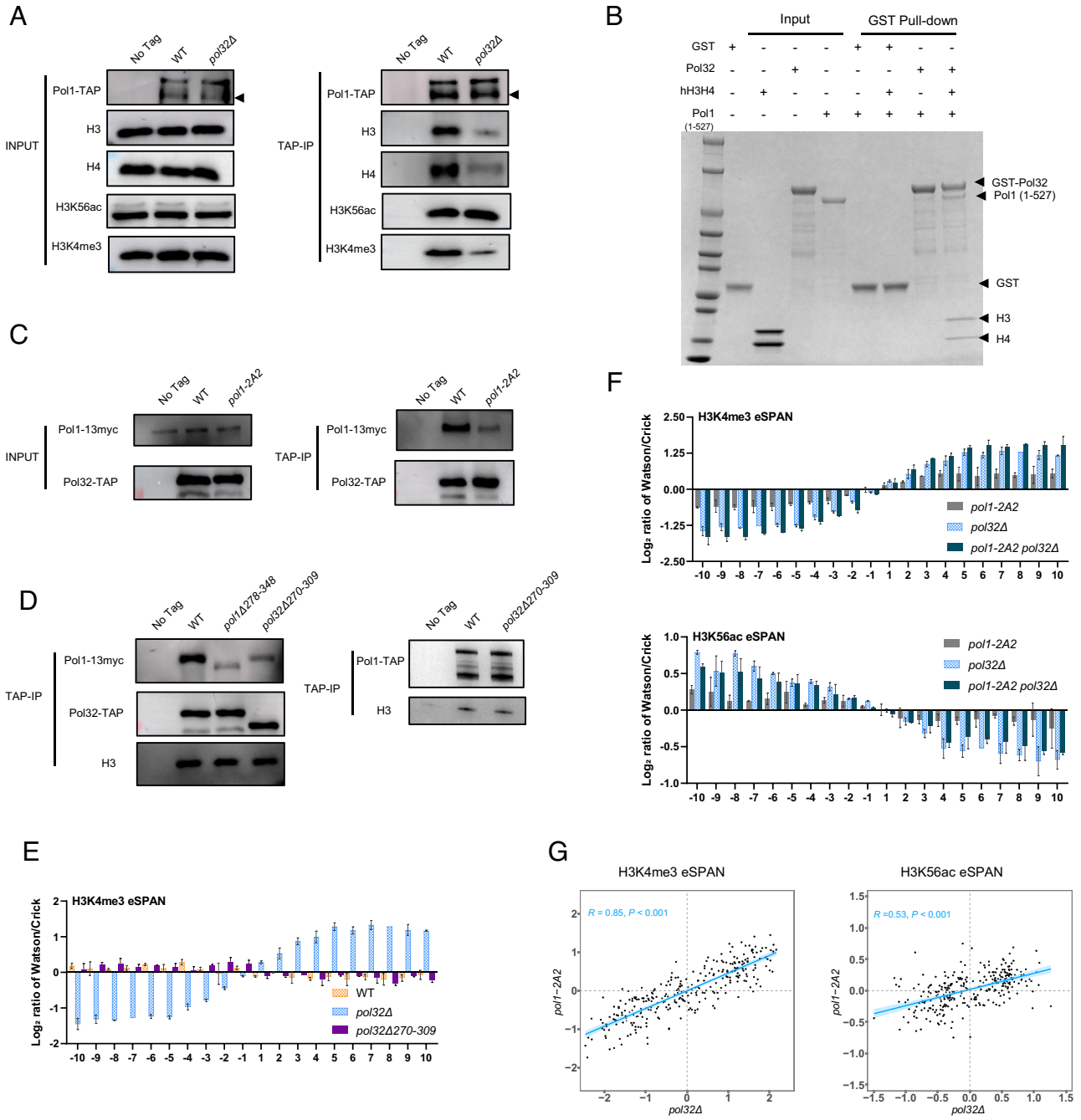

Fig. 3. Pol1 functions as a Pol32-downstream chaperone in the parental histone H3–H4 transfer pathway. (*A*) Analysis of Pol1-TAP-associated proteins from WT and *pol32Δ* cells. (*B*) Pol32–Pol1 (1 to 527a.a.) interaction was enhanced in the presence of H3–H4 tetramers by in vitro binding assay. The beads bearing GST-pol32 or GST (negative control) proteins were first incubated with H3–H4 tetramers, followed by adding Pol1 (1 to 527). The pull-down assay was performed in a buffer containing 300 mM NaCl. (*C*) In vivo analysis of the Pol32–Pol1 interaction by Pol32-TAP purification in WT and *pol1-2A2* mutant cells. (*D*) *pol1Δ278-348* and *pol32Δ270-309* are partial defects in Pol1–Pol32 interaction, but these deletion mutants do not affect their interaction with histone H3. *Left* and *Right* panels are analysis of Pol32-TAP- and Pol1-TAP-associated proteins, respectively. The 278 to 527a.a. of Pol1 and 270 to 309a.a. of Pol32 are reported involved in Pol1–Pol32 interaction (30–32). As 278 to 527a.a. of Pol1 is overlapped with the catalytic core (Pol1-core; 349 to 1,259a.a.) and *Pol1Δ278-527* is lethal, we used a nonessential *pol1Δ278-348* in this assay. Input controls are shown in *SI Appendix*, Fig. S3 *A* and *B*. (*E*) The average bias ratio of H3K4me3 eSPAN signal at each of the nucleosomes flanking the early replication origins in WT, *pol32Δ*, and *pol32Δ*270-309 cells. The data displayed in the box filled with grids have been shown in Fig. 1*A*. (*F*) The average eSPAN bias of H3K4me3 (*Upper*) and H3K56ac (*Lower*) at each nucleosome flanking the early replication origins in *pol1-2A2*, *pol32Δ*, and *pol1-2A2 pol32Δ* cells. The data displayed in the box filled with grids have been shown in Fig. 1*A*. (*G*) The eSPAN bias pattern of H3K4me3 (*Left*) and H3K56ac (*Right*) in *pol32Δ* is correlated with that of *pol1-2A2*.

histone transfer pathway (*SI Appendix*, Fig. S5*D*). Our study unveils the molecular mechanism underlying the parental histone transfer process, a pivotal step in epigenetic inheritance.

Parental histone H3–H4 transfer, a key step in epigenetic inheritance, is intricately regulated by replisome components. There are three DNA polymerases (Pol α, Pol ε, Pol δ) responsible for genomic DNA replication (39, 40). Previously, the leading strand Pol ε subunits (Dpb3/Dpb4) and lagging strand Pol α catalytic subunit (Pol1) have been identified as involved in parental histone H3–H4 recycling (15, 18, 19). In this study, we showed that the Polδ subunit Pol32 is also involved in the recycling of parental histones. Just as mutations in the catalytic domain of DNA polymerases are associated with alterations in DNA replication fidelity, mutations in the chaperones of parental histone transfer are

linked to chromatin instability (3, 41). These findings highlighted the crucial role of DNA polymerase complexes in chromatin replication and epigenetic instability. In the unicellular yeast system, chromatin instability can be frequently observed via loss of silencing at normally repressed loci such as silenced mating-type loci or telomeric regions. Chromatin instability has also been shown to have a role in antifungal drug resistance phenotypes (42). In *Drosophila*, the partition of parental histones plays an important role for germ cell differentiation (43). In mammals, chromatin instability may lead to cell differentiation and embryonic development defects (22, 23). Taken together, the fundamental DNA replication machinery plays a regulatory role in epigenetics inheritance and cell fate determination.

A pivotal question arises regarding why defects in the parental histone transfer process lead to chromatin instability. A "copy and paste" mechanism for histone tail modifications has been proposed to explain epigenetic inheritance (21, 44). The PRC2 complex, a major gene silencer in mammalian cells, binds to the histone tail modification H3K27me3, promoting further local H3K27me3 modifications (45). Similarly, in the absence of demethylase, Clr4 in fission yeast can perform this reader-writer function to replicate H3K9me3 modifications (44). This "read and write" mechanism is executed by PRC2 and Clr4 enzymes. In budding yeast, where H3K27me3 and H3K9me3 modifications are undetectable, current observations do not align with the copy and paste model. In the *dpb3Δ* and *mcm2-3A* mutants, parental histones exhibit a strong leading and lagging strand bias, respectively. Both single mutants display increased chromatin instability compared to wild-type cells (17, 18). For instance, a *dpb3Δ mcm2-3A* double mutant demonstrated an elevated loss of silence frequency relative to single mutants (21), despite sharing a similar parental histone deposition pattern with the WT (GSE240331). In both the previous and current studies, the *mcm2-3A* mutant exhibits a loss of silencing at a level similar to the *pol1-2A2* mutant, despite displaying a substantially higher parental histone bias pattern (19). Notably, *pol32Δ* exhibited a marginal loss of silence frequency but a pronounced parental histone bias pattern compared to the *pol1-2A2* mutant. These observations cannot be easily explained by a simple copy and paste model of histone modification. The minor phenotypic effect of parental histone transfer mutants is understandable, considering the notion that the parental histone transfer pathway is expected to have a profound effect on DNA sequence-independent inheritance, a phenomenon not yet detected in budding yeast. In this study, the identification of a key histone H3–H4 chaperone Pol32, in sequential with Mcm2, provides a promising target for further exploration of the mechanisms underlying epigenetic inheritance by histone chaperones.

Materials and Methods

Yeast Strains. All yeast strains used in this study were W303-1 background except the histone H3-tag switch strains (Cyc565 and cyc1276), which were S228C background (*SI Appendix*, Table S1). Pol1 and Pol32 mutagenesis was performed using the CRISPR/Cas9 plasmid pML104 or pML107 along with dsDNA donor (46), while gene deletion and TAP (Tandem affinity purification)/myc-tag were knock-in using PCR-based methods (47). The oligonucleotides used in this study are listed in *SI Appendix*, Table S2.

eSPAN. We performed eSPAN according to the protocol in our previous studies (16, 17) with some modifications. Briefly, yeast cells were synchronized with alpha-factor and released in yeast extract peptone dextrose (YPD) medium with BrdU (400 μg/mL) following the standard protocol (18). The cells were digested with MNase (New England Biolabs (NEB), Cat# M0247S), after saving 1% for BrdU-IP, the rest of digested chromatin underwent ChIP against H3K4me3 (Abcam, ab8580), H3K56ac (25), HA-Tag (Sigma, Cat#12CA5), or T7-Tag (BETHYL, Cat#A190-117A), individually. Then DNA extracted from the ChIP products was end-repaired and ligated with adapters using the VAHTS® Universal DNA Library Prep Kit for Illumina V3 (Vazyme, Cat#ND607). After saving 1% for ChIP-seq analysis, the remaining products were subjected to BrdU-IP as previously reported (16), and the resulting products were amplified with NEBNext High-Fidelity 2× PCR Master Mix (NEB, Cat# M0541L) and indexing primers. The obtained libraries were sequenced using the paired-end method by the Illumina Nova 6000 platform.

Tandem Affinity Purification Assay for Pol1, Pol32, and Mcm2. Yeast cells were cultured in liquid YPD medium at 30 °C until the OD_{600} reached 1.8 to 2.0, and were harvested by centrifugation. The cell pellets were washed with cold water containing 10% glycerol and resuspended in an equal volume of TAP IP buffer (25 mM Tris pH 8.0, 100 mM NaCl, 10 mM $MgCl_2$, 1 mM ethylenediaminetetraacetic acid, 0.01% NP-40, 1 mM dithiothreitol (DTT), 1 mM phenylmethylsulfonyl fluoride, 1 mM Pefabloc, 1 mM Benzamidine, 15 KU/mL DNase I). Cell resuspensions were lysed using the Mini-Beadbeater-16 (Biospec) at cryogenic conditions with four cycles (30 s on, 1-min off for each). The cell lysate was centrifuged at 20,000 g for 10 min, and the soluble portion was incubated on ice for 30 min with 75 μg/mL ethidium bromide. After centrifugation at 20,000 g for 30 min, the supernatant was mixed with prewashed IgG beads (Cytiva, Cat# 17096901) and incubated at 4 °C for 2 h. The IgG beads were washed three times with TAP IP buffer and then boiled in the SDS sample buffer. Western blot analysis was performed with antibodies against protein A (Proteintech, Cat# 66945-1-Ig), H3 (Abcam, Cat#ab1791), H4 (Proteintech, Cat# 16047-1-AP), H3K56ac (25), H3K4me3 (CST, Cat#9751), and myc-Tag (CST, Cat#2276). The detailed antibody information is displayed in *SI Appendix*, Table S3.

Pol32-Flag Immunoprecipitation Assay. Yeast cells carrying pRS423-Pol32-3×Flag or an empty vector pRS423 control were cultured in synthetic complete medium minus histidine at 30 °C until the OD_{600} reached 1.8 to 2.0. The samples were lysed following the TAP purification assay steps and the supernatant was incubated with prewashed anti-Flag Magnetic Beads (MCE, cat#HY-K0207) at 4 °C for 2 h. After three washes, the beads were boiled in the SDS loading buffer and subjected to western blot analysis with antibodies against Flag (CST, Cat#14793), H3 (Abcam, Cat#ab1791), H4 (Proteintech Cat# 16047-1-AP), H3K56ac (25), H3K4me3 (CST, Cat#9751), and myc-Tag (CST, Cat#2276).

Purification of Recombinant Mcm2, Pol1, and Pol32. Yeast Pol32 and codon-optimized Mcm2 were cloned into the pGEX4T-1 vector to construct GST (glutathioneS-transferase)-tagged Pol32 and Mcm2. The codon-optimized N-terminal of yeast Pol1 (1 to 527 AA) was cloned into the pET28b vector to produce HIS-tagged Pol1. To express these fusion proteins, the plasmids were transformed into the BL21 (DE3) *Escherichia coli* strain (TransGen Biotech, Cat#CD601-02). The transformed cells were cultured in Luria-Bertani medium (Sangon biotech, Cat#A507002-0250) supplemented with 50 μg/mL ampicillin (for pGEX4T-1 vector expression) or 50 μg/mL kanamycin (for pET28b vector expression). The cells were cultured at 37 °C with shaking until OD600 reached 0.8. Expression of these fusion proteins was induced by 0.3 mM IPTG (Isopropyl β-D-1-thiogalactopyranoside) (Sangon biotech, Cat#A600168-0100) at 16 °C for 16 h. Bacterial cells were pelleted by centrifugation at 4,000 rpm for 10 min, resuspended in a lysis buffer containing 20 mM Tris-HCl and 500 mM NaCl, and lysed by a high-pressure homogenizer (ATS company, AH-1500). After centrifugation, the supernatant of the samples was subjected to affinity purification. GST-tagged proteins were purified by Glutathione Resin (GenScript, Cat#L00206-100) and HIS-tagged protein by NI-Charged Resin (GenScript, Cat#L00666-100). In the end, GST-Pol32 and HIS-Pol1 were purified with a gel filtration column (Cytiva, HiLoad 16/600 Superdex 200 column). For GST-Mcm2, purification was accomplished through gel filtration column chromatography following the removal of the GST tag by TEV (Beyotime Biotechnology, Cat#P2310M).

Purification of Recombinant Histone H3.1–H4 Tetramer. The human histones H3.1–H4 tetramers were purified as previously reported (48). The pETDuet-1 vector and BL21 (DE3) were used as the expression vector and host strain, respectively. When the cell culture reached an OD600 of 1.5, 1 mM IPTG was added, and the cells were cultured at 37 °C for an additional 4 h to induce protein expression. The cells were lysed in lysis buffer (1 M NaCl, 20 mM Tris-HCl pH 7.5) and centrifuged to obtain the supernatant. Then, a heparin column was used to capture the H3–H4 tetramer from the supernatant, and a gel filtration column was used for further purification.

GST Pulldown Assays to Detect Pol32–H3–H4, Pol32–Mcm2, and Pol32–Pol1 Interaction. For the pulldown of GST-Pol32 with H3–H4 tetramers, Glutathione Resin (50 μL) was suspended in 200 μL of binding buffer with three different salt concentrations (300, 500, or 750 mM NaCl in 20 mM Tris, pH 7.5). And 1 nmol of GST-Pol32 was added and incubated at 4 °C for 2 h. Then, 1 nmol of H3–H4 tetramer was added and incubated for another 1 h. After incubation, the beads were washed four times with 1 mL of washing buffer (0.5% Triton X-100 in binding buffer). Finally, the sample was prepared by adding 50 μL of protein loading buffer and analyzed with sodium dodecyl-sulfate polyacrylamide gel electrophoresis (SDS-PAGE) gel and Coomassie Blue staining (Kyr Biotechnology, Cat#18.001.500).

To test the effect of H3–H4 tetramers on the Pol32–Mcm2 interaction, Glutathione Resin (50 μL) was suspended in 200 μL of binding buffer (20 mM Tris, pH 7.5, and 500 mM NaCl) and 1 nmol of GST-Pol32 was added and incubated at 4 °C for 2 h. At the same time, Mcm2 was incubated with H3–H4 tetramers at 500 mM NaCl for 1 h to form the Mcm2-H3–H4 complex. Then, 1 nmol of Mcm2 or the Mcm2-H3–H4 complex was added to the Pol32-beads mixture and incubated for an additional 1 h. After incubation, the beads were washed four times with 1 mL of washing buffer (0.5% Triton X-100 in binding buffer). Finally, the sample was prepared by adding 50 μL protein loading buffer and analyzed with SDS-PAGE gel and Coomassie Blue staining.

To test the effect of H3–H4 tetramer on the Pol32–Pol1 interaction, Glutathione Resin (50 μL) was suspended in 200 μL of binding buffer (20 mM Tris, pH 7.5, and 300 mM NaCl), and 1 nmol of GST-Pol32 was added and incubated at 4 °C for 2 h. Then, 1 nmol of H3–H4 tetramers was added to the experimental sample or not, and was incubated for another 1 h. After washing three times with 1 mL of washing buffer, 1 nmol Pol1 was added to the Pol32–H3–H4-beads mixture or Pol32-beads mixture, respectively, and incubated for 1 h. Unbound proteins in the system were washed again using washing buffer. Finally, the sample was prepared by adding 50 μL loading buffer and analyzed with SDS-PAGE gel and Coomassie Blue staining.

To analyze the effect of DNA on the interaction between Pol32 and H3–H4, two complementary ssDNA oligonucleotides were synthesized by Rui Biotech (Beijing, China) and annealed to form a 58 bp dsDNA. The oligos are listed in *SI Appendix*, Table S2. Then Glutathione Resin beads (50 μL) were suspended in 200 μL of binding buffer (20 mM Tris, pH 7.5, and 300 mM NaCl), and 1 nmol of GST-Pol32 was added and incubated at 4 °C for 2 h. Then the 58 bp dsDNA with gradient concentration was added and incubated for another 1 h. After washing three times with 1 mL of washing buffer, 1 nmol H3–H4 was added to each DNA-Pol32 mixture respectively and the mixture was incubated for 1 h. Unbound H3H4 in the system were washed again using washing buffer. Finally, the sample was prepared by adding 50 μL loading buffer and analyzed with SDS-PAGE gel and Coomassie Blue staining.

Electrophoretic Mobility Shift Assay to detect Pol32–DNA Interaction. GST-Pol32 was incubated with a 58 bp dsDNA in assembly buffer (20 mM Tris pH 7.5, 150 mM NaCl, and 1 mM DTT) for 30 min at room temperature. Then, the Pol32–DNA mixtures were separated on a 5% Polyacrylamide gel, prepared as previously reported at 40 V for 120 min at 4 °C (49). The gel was visualized using SYBR Safe DNA stain (Thermo Fisher Scientific, Cat#S33102).

Yeast Spot Assay. Freshly cultured yeast cells were diluted to an optical density at 600 nm (A600) of 0.6. Subsequently, a 10-fold serial dilution was executed, and the cells were spotted onto standard growth medium with or without the specified concentration of the drug agent (YPD+20 or 50 μM HU or 4 or 10 μg/mL CPT). Images were captured at various time points, and representative images are presented.

Analysis of Silencing-Loss at the *HML* Locus. To measure the effect of Pol32 deletion on chromatin state, we analyzed the silencing-loss rate at the *HML* locus in both wild-type and *pol32Δ* strains using the CRASH (Cre-reported altered states of heterochromatin) assay according to a previously published protocol (17). Briefly, 10 colonies of wild-type and *pol32Δ* strains were individually cultivated in YPD medium until the stationary phase. Subsequently, they were diluted to OD600 = 0.01 in YPD, and cultured for another 5 h at 30 °C. We collected 50,000 events for each colony using a BD cytometer. The silencing-loss rate at the HML locus was indicated with the ratio of GFP+/Total cells.

Data Analysis. The sequence mapping and analysis for BrdU-IP-ssSeq and eSPAN were conducted following procedures similar to our previously published work (16, 17). Sequenced reads were mapped to the reference genome of *Saccharomyces cerevisiae* (sacCer3) with Bowtie2 software (50). Only paired-end reads correctly mapped on both sides were selected for further analysis. Following the reference genome, the Watson and Crick strand reads were separated using in-house Perl programs. BEDTools (51) and self-developed Perl programs were used to calculate the genome-wide read coverage.

In order to calculate the average bias of each nucleosome, the eSPAN reads at each nucleosome surrounding the 134 early DNA replication origins were individually counted and assigned to their respective nucleosome positions (52). Following normalization against the corresponding BrdU-IP-ssSeq, the average bias pattern of eSPAN was calculated as $\log_2$ (Watson strand reads/ Crick strand reads) at each nucleosome position. Similarly, $\log_2$ (Lagging strand reads/ Leading strand reads) at each nucleosome position of each of the 134 early replication origins was used to analyze the bias pattern of eSPAN peaks at each origin.

Data, Materials, and Software Availability. The deep sequencing data generated in this study have been deposited in the Gene Expression Omnibus (GEO) database under accession code GSE252049 (53).

ACKNOWLEDGMENTS. This work was supported by the following Fundings. National Key R&D Program of China (2023YFA0913400 to H.G.), the Major Program of the National Natural Science Foundation of China (32090031 to H.G.), the Strategic Priority Research Program of the Chinese Academy of Sciences (XDB0480000 to H.G.), the General Program of the National Natural Science Foundation of China (32070610 to H.G.), NIH grant R01GM130588 (to C.Y.), the Hormel Startup Fund (to C.Y.), the National Natural Science Foundation of China for Young Scholars (32100460 to J.Z. and 32101178 to Y.Y.), the Guangdong Province Fund for Distinguished Young Scholars (2021B1515020109 to H.G.), Shenzhen Institute of Synthetic Biology Scientific Research Program (JCHZ20200005, DWKF20210001, ZTXM20190019 to H.G.), Shenzhen Medical Research Funds (B2302049 to H.G.).

Author affiliations: [a]Shenzhen Key Laboratory of Synthetic Genomics, Guangdong Provincial Key Laboratory of Synthetic Genomics, Key Laboratory of Quantitative Synthetic Biology, Shenzhen Institute of Synthetic Biology, Shenzhen Institute of Advanced Technology, Chinese Academy of Sciences, Shenzhen 518055, China; [b]Department of Biotherapy, Cancer Center and State Laboratory of Biotherapy, and Frontiers Science Center for Disease-related Molecular Network, West China Hospital, Sichuan University, Chengdu, Sichuan Province 610041, China; [c]Hormel Institute, University of Minnesota, Austin, MN 55912; [d]College of Veterinary Medicine, South China Agricultural University, Guangzhou, Guangdong 510642, China; [e]Cancer Centre, Faculty of Health Sciences, University of Macau, Macau, China; [f]School of Life Sciences, Henan University, Kaifeng 475004, China; [g]Shenzhen Research Institute of Henan University, Shenzhen 518000, China; [h]Kobilka Institute of Innovative Drug Discovery, School of Medicine, Chinese University of Hong Kong, Shenzhen 518172, China; [i]Cold Spring Harbor Laboratory, Cold Spring Harbor, NY 11724; [j]Pathology and Pathophysiology Basic Medical School, Qingdao University, Qindao 266000, China; [k]Department of Biomedical Sciences, City University of Hong Kong, Hong Kong Special Administration Region, China; [l]Key Laboratory of Biochip Technology, Biotech and Health Centre, Shenzhen Research Institute of City University of Hong Kong, Shenzhen 518172, China; and [m]Division of Critical Care Medicine, Department of Pediatrics, Stanford University School of Medicine, Stanford, CA 94305

1. P. Chen, W. Li, G. Li, Structures and functions of chromatin fibers. *Annu. Rev. Biophys.* **50**, 95–116 (2021).
2. R. Margueron, D. Reinberg, Chromatin structure and the inheritance of epigenetic information. *Nat. Rev. Genet.* **11**, 285–296 (2010).
3. T. M. Escobar, A. Loyola, D. Reinberg, Parental nucleosome segregation and the inheritance of cellular identity. *Nat. Rev. Genet.* **22**, 379–392 (2021).
4. L. Louters, R. Chalkley, Exchange of histones H1, H2A, and H2B in vivo. *Biochemistry* **24**, 3080–3085 (1985).
5. H. Kimura, P. R. Cook, Kinetics of core histones in living human cells: Little exchange of H3 and H4 and some rapid exchange of H2B. *J. Cell Biol.* **153**, 1341–1353 (2001).
6. M. Radman-Livaja *et al.*, Patterns and mechanisms of ancestral histone protein inheritance in budding yeast. *PLoS Biol.* **9**, e1001075 (2011).
7. M. Xu *et al.*, Partitioning of histone H3-H4 tetramers during DNA replication-dependent chromatin assembly. *Science* **328**, 94–98 (2010).
8. R. J. Burgess, Z. Zhang, Histone chaperones in nucleosome assembly and human disease. *Nat. Struct. Mol. Biol.* **20**, 14–22 (2013).

9. A. Serra-Cardona, Z. Zhang, Replication-coupled nucleosome assembly in the passage of epigenetic information and cell identity. *Trends Biochem. Sci.* **43**, 136–148 (2018).
10. S. Svikovic, J. E. Sale, The effects of replication stress on S phase histone management and epigenetic memory. *J. Mol. Biol.* **429**, 2011–2029 (2017).
11. T. H. Huang *et al.*, The histone chaperones ASF1 and CAF-1 promote MMS22L-TONSL-mediated Rad51 loading onto ssDNA during homologous recombination in human cells. *Mol. Cell* **69**, 879–892.e5 (2018).
12. C. C. Chen *et al.*, Acetylated lysine 56 on histone H3 drives chromatin assembly after repair and signals for the completion of repair. *Cell* **134**, 231–243 (2008).
13. M. Foltman *et al.*, Eukaryotic replisome components cooperate to process histones during chromosome replication. *Cell Rep.* **3**, 892–904 (2013).
14. H. Huang *et al.*, A unique binding mode enables MCM2 to chaperone histones H3–H4 at replication forks. *Nat. Struct. Mol. Biol.* **22**, 618–626 (2015).
15. N. Petryk *et al.*, MCM2 promotes symmetric inheritance of modified histones during DNA replication. *Science* **361**, 1389–1392 (2018).
16. C. Yu *et al.*, Strand-specific analysis shows protein binding at replication forks and PCNA unloading from lagging strands when forks stall. *Mol. Cell* **56**, 551–563 (2014).
17. C. Yu *et al.*, A mechanism for preventing asymmetric histone segregation onto replicating DNA strands. *Science* **361**, 1386–1389 (2018).
18. H. Gan *et al.*, The Mcm2-Ctf4-Polalpha axis facilitates parental histone H3–H4 transfer to lagging strands. *Mol. Cell* **72**, 140–151.e3 (2018).
19. Z. Li *et al.*, DNA polymerase alpha interacts with H3–H4 and facilitates the transfer of parental histones to lagging strands. *Sci. Adv.* **6**, eabb5820 (2020).
20. C. Evrin, J. D. Maman, A. Diamante, L. Pellegrini, K. Labib, Histone H2A–H2B binding by Pol alpha in the eukaryotic replisome contributes to the maintenance of repressive chromatin. *EMBO J.* **37**, e99021 (2018).
21. D. S. Saxton, J. Rine, Epigenetic memory independent of symmetric histone inheritance. *Elife* **8**, e51421 (2019).
22. A. Wenger *et al.*, Symmetric inheritance of parental histones governs epigenome maintenance and embryonic stem cell identity. *Nat. Genet.* **55**, 1567–1578 (2023).
23. Q. Wen *et al.*, Symmetric inheritance of parental histones contributes to safeguarding the fate of mouse embryonic stem cells during differentiation. *Nat. Genet.* **55**, 1555–1566 (2023).
24. X. Xu, X. Hua, K. Brown, X. Ren, Z. Zhang, Mcm2 promotes stem cell differentiation via its ability to bind H3–H4. *Elife* **11**, e80917 (2022).
25. J. Han *et al.*, Rtt109 acetylates histone H3 lysine 56 and functions in DNA replication. *Science* **315**, 653–655 (2007).
26. H. Masumoto, D. Hawke, R. Kobayashi, A. Verreault, A role for cell-cycle-regulated histone H3 lysine 56 acetylation in the DNA damage response. *Nature* **436**, 294–298 (2005).
27. H. Zhou, B. J. Madden, D. C. Muddiman, Z. Zhang, Chromatin assembly factor 1 interacts with histone H3 methylated at lysine 79 in the processes of epigenetic silencing and DNA repair. *Biochemistry* **45**, 2852–2861 (2006).
28. K. F. Verzijlbergen *et al.*, Recombination-induced tag exchange to track old and new proteins. *Proc. Natl. Acad. Sci. U.S.A.* **107**, 64–68 (2010).
29. A. C. Simon *et al.*, A Ctf4 trimer couples the CMG helicase to DNA polymerase alpha in the eukaryotic replisome. *Nature* **510**, 293–297 (2014).
30. E. Johansson, P. Garg, P. M. Burgers, The Pol32 subunit of DNA polymerase delta contains separable domains for processive replication and proliferating cell nuclear antigen (PCNA) binding. *J. Biol. Chem.* **279**, 1907–1915 (2004).
31. F. C. Gray, J. R. Pohler, E. Warbrick, S. A. MacNeill, Mapping and mutation of the conserved DNA polymerase interaction motif (DPIM) located in the C-terminal domain of fission yeast DNA polymerase delta subunit Cdc27. *BMC Mol. Biol.* **5**, 21 (2004).
32. M. E. Huang, B. Le Douarin, C. Henry, F. Galibert, The Saccharomyces cerevisiae protein YJR043C (Pol32) interacts with the catalytic subunit of DNA polymerase alpha and is required for cell cycle progression in G2/M. *Mol. Gen. Genet.* **260**, 541–550 (1999).
33. N. Acharya, R. Klassen, R. E. Johnson, L. Prakash, S. Prakash, PCNA binding domains in all three subunits of yeast DNA polymerase delta modulate its function in DNA replication. *Proc. Natl. Acad. Sci. U.S.A.* **108**, 17927–17932 (2011).
34. J. Ji, X. Tang, W. Hu, K. A. Maggert, Y. S. Rong, The processivity factor Pol32 mediates nuclear localization of DNA polymerase delta and prevents chromosomal fragile site formation in Drosophila development. *PLoS Genet.* **15**, e1008169 (2019).
35. M. E. Huang, A. G. Rio, M. D. Galibert, F. Galibert, Pol32, a subunit of Saccharomyces cerevisiae DNA polymerase delta, suppresses genomic deletions and is involved in the mutagenic bypass pathway. *Genetics* **160**, 1409–1422 (2002).
36. K. J. Gerik, X. Li, A. Pautz, P. M. Burgers, Characterization of the two small subunits of Saccharomyces cerevisiae DNA polymerase delta. *J. Biol. Chem.* **273**, 19747–19755 (1998).
37. T. van Welsem *et al.*, Synthetic lethal screens identify gene silencing processes in yeast and implicate the acetylated amino terminus of Sir3 in recognition of the nucleosome core. *Mol. Cell Biol.* **28**, 3861–3872 (2008).
38. A. E. Dodson, J. Rine, Heritable capture of heterochromatin dynamics in Saccharomyces cerevisiae. *Elife* **4**, e05007 (2015).
39. Z. X. Zhou, S. A. Lujan, A. B. Burkholder, M. A. Garbacz, T. A. Kunkel, Roles for DNA polymerase delta in initiating and terminating leading strand DNA replication. *Nat. Commun.* **10**, 3992 (2019).
40. S. A. Nick McElhinny, D. A. Gordenin, C. M. Stith, P. M. Burgers, T. A. Kunkel, Division of labor at the eukaryotic replication fork. *Mol. Cell* **30**, 137–144 (2008).
41. J. D. Strauss, Z. F. Pursell, Replication DNA polymerases, genome instability and cancer therapies. *NAR Cancer* **5**, zcad033 (2023).
42. V. N. Nikolov, D. Malavia, T. Kubota, SWI/SNF and the histone chaperone Rtt106 drive expression of the Pleiotropic Drug Resistance network genes. *Nat. Commun.* **13**, 1968 (2022).
43. M. Wooten, R. Ranjan, X. Chen, Asymmetric histone inheritance in asymmetrically dividing stem cells. *Trends Genet.* **36**, 30–43 (2020).
44. K. Ragunathan, G. Jih, D. Moazed, Epigenetic inheritance uncoupled from sequence-specific recruitment. *Science* **348**, 1258699 (2015).
45. K. H. Hansen *et al.*, A model for transmission of the H3K27me3 epigenetic mark. *Nat. Cell Biol.* **10**, 1291–1300 (2008).
46. M. F. Laughery *et al.*, New vectors for simple and streamlined CRISPR-Cas9 genome editing in Saccharomyces cerevisiae. *Yeast* **32**, 711–720 (2015).
47. C. Noguchi, M. V. Garabedian, M. Malik, E. Noguchi, A vector system for genomic FLAG epitope-tagging in Schizosaccharomyces pombe. *Biotechnol. J.* **3**, 1280–1285 (2008).
48. C. M. Hammond *et al.*, DNAJC9 integrates heat shock molecular chaperones into the histone chaperone network. *Mol. Cell* **81**, 2533–2548.e9 (2021).
49. M. Seo, L. Lei, M. Egli, Label-free electrophoretic mobility shift assay (EMSA) for measuring dissociation constants of protein-RNA complexes. *Curr. Protoc. Nucleic Acid Chem.* **76**, e70 (2019).
50. B. Langmead, C. Wilks, V. Antonescu, R. Charles, Scaling read aligners to hundreds of threads on general-purpose processors. *Bioinformatics* **35**, 421–432 (2019).
51. A. R. Quinlan, BEDTools: The Swiss-army tool for genome feature analysis. *Curr. Protoc. Bioinform.* **47**, 11–34 (2014).
52. K. Brogaard, L. Xi, J. P. Wang, J. Widom, A map of nucleosome positions in yeast at base-pair resolution. *Nature* **486**, 496–501 (2012).
53. H. Gan *et al.*, Next-generation sequencing datasets. National Center for Biotechnology Information Gene Expression Omnibus (NCBI GEO). http://www.ncbi.nlm.nih.gov/geo/query/acc.cgi?acc=GSE252049. Deposited 26 December 2023.